The Second International Conference on Integrated Micro Nanotechnology for Space Applications (MNT99), Pasadena, CA, April 11-15, 1999

MICROTHRUSTERS FOR NANOSATELLITES

Siegfried W. Janson, Henry Helvajian, William W. Hansen and Lt. John Lodmell*
Center for Microtechnology, Technology Operations, The Aerospace Corporation

** U.S. Air Force Space and Missile Systems Center, Temporarily on assignment to The Aerospace Corporation*

Abstract

Batch-fabrication technology developed for the semiconductor industry can be modified to produce "smaller, faster, cheaper" mechanical and electromechanical systems. These microelectromechanical systems (MEMS) include fluid valves, fluid pumps, accelerometers, gyros, chemical sensors, scanning micromirrors, and electromechanical switches. Semiconductor batch-fabrication techniques, combined with laser machining, can produce low-cost chemical and electric MEMS microthruster systems for nanosatellites and microsatellites. Basic propulsion requirements for these spacecraft are presented and compared to what a MEMS cold-gas, resistojet, solid thruster array, or ion engine system could deliver. We have constructed a 1-cm-scale cold-gas bi-directional thruster module, several sub-cm-scale resistojets, arrays of single-shot "digital" thrusters, and test structures for field emission and field ionization-based ion engines. The cold-gas thruster module uses commercially available MEMS silicon microvalves mounted to custom laser-machined glass nozzles and structure. The microresistojets were fabricated with a standard CMOS processes followed by an anisotropic etch to create the flow channels, plenum, and nozzle. CMOS-compatibility enables the fabrication of thrusters, flow sensors, temperature sensors, and control electronics on the same substrate to produce a thruster system "on a chip". The digital thruster arrays, fabricated for a DARPA-sponsored MEMS program, are composed of two silicon micromachined layers and one micromachined glass layer. Conventional integrated circuit manufacturing techniques are used to create one of the silicon layers, and laser machining is used on the other two layers. Thrust, minimum impulse bit, and specific impulse are presented for the cold gas, resistojet, and digital thrusters.

1. INTRODUCTION

Batch-fabrication of microelectromechanical systems (MEMS) initiated a revolution that brought sensing and actuation to microelectronic systems; microcircuits can now monitor and directly interact with their immediate physical, chemical, and biological environment. Integration of sensors, actuators, and control electronics at the die or semiconductor substrate level results in higher reliability and reduced cost, a reduction in the number of piece-parts, elimination of manual assembly steps, better control of material variability, reduced mass, and reduced power requirements. Researchers at the Aerospace Corporation, NASA's Jet Propulsion Laboratory, and the European Space Agency have investigated emerging microtechnologies and determined how they will impact future space systems.[1,2,3,4,5,6,7] Examples of MEMS and microsystems that can be incorporated in spacecraft include inertial measurement units, Earth sensors, and micropropulsion systems.

2. MICROPROPULSION REQUIREMENTS

Table 1 shows representative in-plane and out-of-plane maneuvers, their associated velocity increment (ΔV or "delta V"), and the minimum thrust required per kg of spacecraft mass for two different maneuver times. Thrusting time is also given in Table 1 because many propulsive maneuvers such as changing orbit inclination are efficient over only part of the orbit. With the exception of rapid

inclination change, 1-kg class nanosatellites require 10-to-1000 μN thrusters and 10-kg microsatellites require 0.1-to-10 mN thrusters for on-orbit maneuvering.

Table 1. Propulsion requirements for representative missions. GEO is geosynchronous Earth orbit.

Mission	Mission Time	Thrusting Time	ΔV (m/s)	Thrust (μN/ kg)
Increase altitude from 700 km to 701 km	0.82 hours (half orbit)	10 min.	0.53	880
	2 days	2 days	0.53	3.1
Move 10 km ahead at 700 km altitude	3.3 hr. (two orbits)	40 min.	1.1	460
	2 days	40 min.	0.04	17
Change inclination by 1^o at 700 km altitude	0.82 hours (half orbit)	10 min.	131	220,000
	2 days	12 hours	131	3,000
De-orbit from 700 km (Hohmann transfer)	0.80 hours (half orbit)	10 min.	160	270,000
De-orbit from 700 km (Low-Thrust Spiral)	1 week	1 week	330	550
Change inclination by 1^o at GEO	12 hours (half orbit)	10 min.	54	9,000
	1 week	1.75 days	54	360
North-South Station-Keeping at GEO	1 week	20 min.	0.96	800
Boost altitude by 100 km at GEO	12 hours (half orbit)	10 min.	3.65	6,100
	1 week	1 week	3.65	6

One of the more interesting applications of mass-produced satellites is to keep them together in a "local cluster" to simulate operation of a much larger spacecraft. The basic concept is to start with a reference orbit for the center of the cluster and add spacecraft in a single plane (the "cluster plane") whose normal is inclined 60^o from the reference orbit normal in the direction towards the instantaneous nadir (see Fig. 1). This orbital configuration was proposed over a decade ago to allow multiple geostationary satellites to share a common orbital "slot".[8,9]

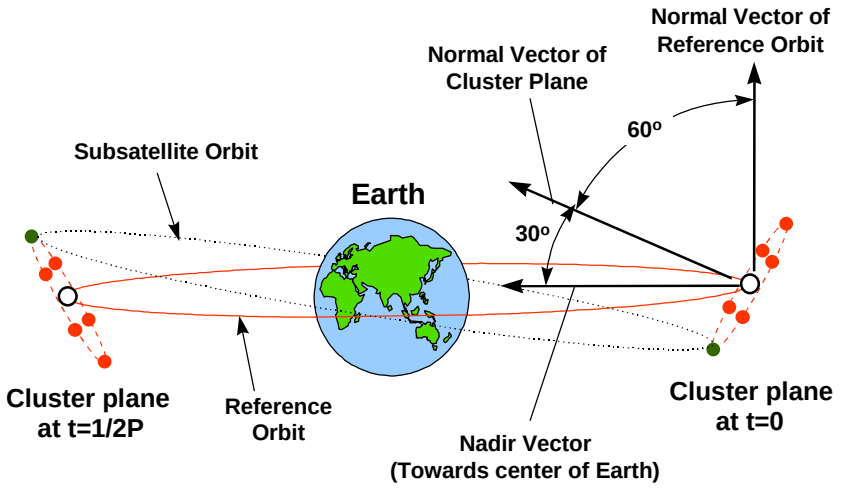

Figure 1. Geometry of the sparse array orbital configuration. P is the orbital period.

The semi-major axes of all "subsatellites" are almost identical to the semi-major axis of the reference orbit in order to keep the orbital periods equal. As seen from Earth, the subsatellites orbit about the center of the cluster once per cluster orbit period about the Earth. To first order, there is no radial motion of subsatellites within the cluster plane and the system appears to rotate as a rigid body. The net result is that an arbitrary distribution of spacecraft in this plane will maintain its configuration within the plane, and this plane will rotate about the Earth such that its normal is always pointing towards the Earth, 30^o above or below the reference orbit plane. Hundreds-to-thousands of physically disconnected small spacecraft can occupy this plane and simulate operation of kilometer-scale and larger spacecraft.

The second and higher-order terms in the Earth's gravitational potential, solar pressure, and atmospheric drag conspire to disperse local clusters, but the first and last effects decrease rapidly with altitude. An efficient orbit maintenance or formation-keeping strategy developed at the Aerospace Corporation relies on selection of a so-called "frozen orbit"[10] for the reference orbit and use of multiple thruster micro-corrections for each subsatellite per orbit.[11] Frozen orbits minimize variations in eccentricity and argument of perigee caused by higher-order gravitational harmonics (the lumpiness of the Earth's gravity field). The micro-corrections occur along in-track and cross-track directions and are computed using an auto-feedback controller based on instantaneous relative position and velocity deviations. Average micro-correction impulse bits are 1.3-mN-s for a satellite at 1-km radius within a local cluster orbiting at 700-km; the yearly formation-keeping requirement can be kept below 24-m/s for all satellites in this cluster. Required minimum impulse bits are in the 10's-of-μN-s range. The key to reducing formation-keeping propulsion requirements is to measure relative position and velocity with high accuracy; the previous propulsion requirements were based on a position measurement accuracy of 10-cm and a velocity measurement accuracy of 1-mm/s. Under these conditions, the satellites stay within 20-meters of their ideal locations within the cluster.

To reduce small spacecraft complexity and cost, thrusters may also be used for active attitude control in lieu of momentum wheels and magnetic torque rods. For constant density and geometric configuration, moments of inertia scale as s^5 (the mass M scales as s^3 and the moment of inertia scales as Ms^2) where s is a characteristic satellite dimension. The applied torque scales as Fs where F is the thrust applied a distance s from the center-of-mass. Thrust required to produce a fixed angular acceleration therefore scales as s^4, which drastically reduces attitude control ΔV requirements as spacecraft shrink. Figure 2 shows calculated thrust levels and ΔV requirements to slew a disk-shaped, 1-kg mass, 12-cm diameter spacecraft of constant density (moment-of-inertia = 0.0018-kg-m^2) 90^o about the cylindrical axis using 2 thrusters mounted on opposite ends of a diameter to produce a torque couple. The thrust level in Fig. 2 is per thruster while the ΔV is for the entire slew maneuver. Slew times of about 10-s are considered fairly fast, while slew times greater than 1000-s would be too slow for many applications.

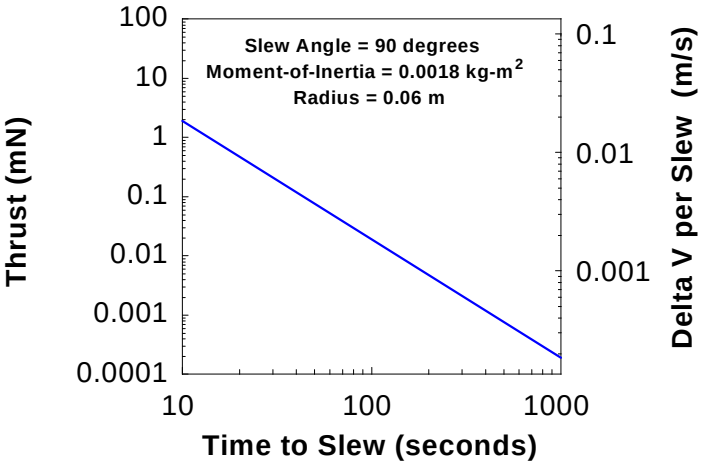

Figure 2. Force and velocity increment required to change angular orientation of a 1-kg mass, 12-cm diameter solid silicon spacecraft by 90^o as a function of maneuver time.

Thrust levels between 0.001-and-1-mN are adequate for nanosatellite attitude control. Attitude control velocity increments must be calculated from actual mission requirements, but an upper range can be estimated by assuming five moderately fast (30-s time-scale) 90^o slews per orbit. With orbit periods about 100-minutes in LEO, one obtains an average thrust level of 100-μN and a ΔV of ~170-m/s/year. For the local cluster case where three slow (100-s) 45^o slews may be required per orbit to fire formation-keeping thrusters, one obtains an average thrust of 5-μN and an attitude control ΔV of ~10 m/s/year.

In general, nanosatellites will require propulsion systems that can deliver average thrust levels somewhere between 1- and 1000-μN for orbit insertion, orbit maintenance, and attitude control. Minimum impulse bits of 1-to-100 μN-s or smaller are desirable, but this will be dictated by specific mission requirements such as position and pointing accuracy. Mission ΔV requirements can range from 10-to-1000 m/s depending on expected on-orbit lifetime, mission strategy, and disposal requirements. For a 1-km radius local cluster in LEO with a 5-year mission life, the ΔV can be about 150-m/s (5 years of formation keeping plus attitude control, negligible drag make-up at 700-km altitude, on-orbit disposal).

3. MICROTHRUSTER SYSTEMS AND SCALING ISSUES

How does one build propellant tanks, propellant lines, valves, etc. using batch-fabrication techniques? One solution is to bond several micromachined layers together so that thin surface cavities become tubes and large cavities become propellant tanks. Figure 3 shows a basic propulsion system concept where three layers are bonded together to form a propellant tank, associated plumbing, and simple expansion nozzles. MEMS valves, pumps, flow monitors, and temperature sensors have already been demonstrated by a number of researchers.[12,13,14,15,16,17] MEMS thrusters are less mature, but significant research and development efforts have been initiated. Recent microthruster reviews can be found in References 18, 19 and 20, and MEMS thruster development in the USA is currently underway at The Aerospace Corporation, TRW, NASA-JPL, MIT, CalTech, and the NASA-Lewis Research Center.[21,22,23,24]

Table 2 lists relevant properties and possible scaling issues for a number of thrusters that are used on-orbit today. The top six devices are gasdynamic while the last two are electrostatic thrusters that use space-charge or externally-applied electric fields to accelerate positive ions in a plasma to energies of several hundred eV and higher. Note that the last four devices in Table 2 are electric thrusters.

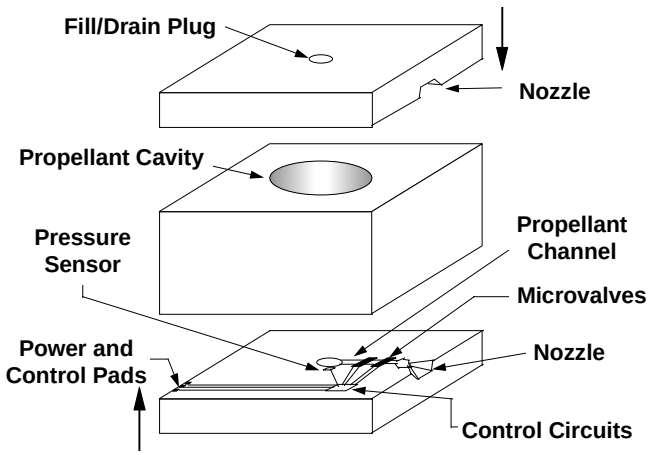

Figure 3. Schematic assembly of a dual thruster micropropulsion system based on microfabrication techniques.

Table 2. Propellants, specific impulse, and scaling issues (to small size) for typical on-orbit thrusters.

Thruster Type	Class	Specific Impulse	Typical Propellants	Micro-scaling Issues
Cold Gas	Chemical	40 – 80 s	Freons, N_2, Ar	Drag losses
Monopropellant	Chemical	180 – 220 s	N_2H_4, H_2O_2	Drag losses
Bipropellant	Chemical	300 – 450 s	N_2H_4+ N_2O_4, H_2 + O_2	Propellant mixing, high flame temperatures
Solid	Chemical	100 - 290 s	Nitocellulose + Nitroglycerine	Ignition
Resistojet	Electric	150 – 330 s	H_2O, NH_3, N_2H_4	Drag losses
Arcjet	Electric	400 – 900 s	NH_3, N_2H_4	Electrode erosion
Hall Effect	Electric	1400 – 2000 s	Xe, Kr	Plasma containment
Ion Engine	Electric	1600 – 5000 s	Xe, Kr	Plasma containment

Not all conventional thrusters can be scaled to small size or thrust level. Cold gas, monopropellant, solid, and resistojet thrusters are readily scaleable to millinewton thrust levels albeit at a cost in performance due to viscous losses. Serious degradation in specific impulse, for example, has been observed in two-dimensional cold gas nozzles with a throat width of 37.5 microns when internal Reynold's numbers drop below 1500.[25] Bipropellant thrusters with millinewton thrust levels can be built, but there are physical limits on how small combustion chambers can be. The chamber volume must be large enough to allow for evaporation (i.e. for liquid propellants), gas mixing and complete combustion. Some combination of pre-mixing propellants, use of highly reactive propellants, micromachined injectors, and high-pressure operation can be used to accelerate the combustion, but fundamental bimolecular reaction rates dictate the necessary reaction zone and thus the volume. In addition, bipropellant thrusters typically operate at stagnation temperatures in excess of 2000 K to obtain high specific impulse, which would melt a silicon combustion chamber.

Micromachined hydrazine monopropellant thrusters may provide moderate specific impulse with high density, low-pressure propellant storage. The specific impulse of conventional hydrazine thrusters is ~220 s which results from an exothermic catalytic decomposition of N_2H_4 into H_2, N_2, and NH_3. Typical gas temperatures are ~1200 K with ammonia fractions of ~20% (M ~ 13).[26] This gas temperature is below the melting point of silicon (1700 K) and silicon dioxide (2000 K) which makes a silicon thruster possible. The remaining engineering problems are to produce a micromachined structure for the catalyst (Shell 405 pellets are used in macroscopic thrusters) and to produce a silicon oxide or other insulation layer in the plenum and throat that will not erode or crack due to thermal stress.

Conventional Hall effect thrusters and ion engines are difficult to scale to small size because magnetic confinement, which is necessary for efficient operation, does not scale favorably with size. Plasmas constantly lose ions and electrons through diffusion across magnetic field lines and most plasma devices are governed by Bohm diffusion where the diffusion coefficient D_B is given by:[27]

$$D_B = KT_e/16eB \quad (1)$$

where K is Boltzmann's constant, T_e is the electron temperature, e is the charge of an electron, and B is magnetic field strength. For a plasma cylinder of radius R, the plasma decays exponentially in time where the time constant τ is given by

$$\tau = R^2/2D_B \quad (2)$$

Substituting Eq. (1) into Eq. (2) shows that the decay time is proportional to R^2B for a constant electron temperature. Shrinking a conventional 20-cm diameter ion engine down to 1 cm diameter

will require magnetic field strengths 400 times higher if plasma decay rate, and approximate containment efficiency, is to be maintained. This is impractical without resorting to superconducting magnetic field coils. Simple numerical analyses of plasma confinement in conventional ring cusp ion engines performed at the Massachusetts Institute of Technology generated similar concerns for ion engine downsizing.[28] Electrostatic microthrusters should be based on ion sources that do not utilize magnetically confined plasmas.

4. A COLD GAS MICROTHRUSTER

The simplest microthruster one can build is a cold gas thruster. We used direct-write laser machining of Foturan™ to fabricate 3D axisymmetric exit nozzles for a 1-mN-class thruster.[29] Foturan is a bulk UV-photosensitive glass/ceramic material manufactured by Schott Glassworks of Germany.[30] Figure 4 shows two optical microscope views of an example nozzle. The nozzle shape and expansion ratio are under user control, and hundreds of nozzles with various characteristics have been produced. The nozzle in Fig. 4 has a throat diameter of 100-microns and an expansion ratio (exit plane area divided by the throat cross-sectional area) of 10:1. Two nearly identical nozzles were used to fabricate the bi-directional cold gas microthruster module shown in Fig. 5. This module integrates laser-processed Foturan parts with two commercially available (circa 1996) MEMS valves (EG&G IC Sensors Corp. Model 4425-15) that are 4-mm-square. Each valve is directly coupled to an exit nozzle and both valves share a common gas plenum.

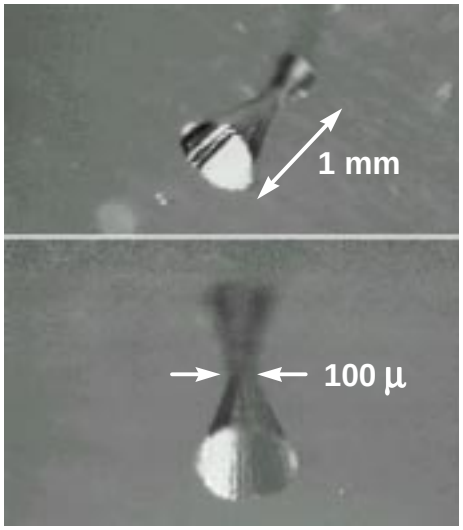

Figure 4. Photo of a laser-machined converging/diverging nozzle in Foturan. *(Aerospace Corp. photo)*

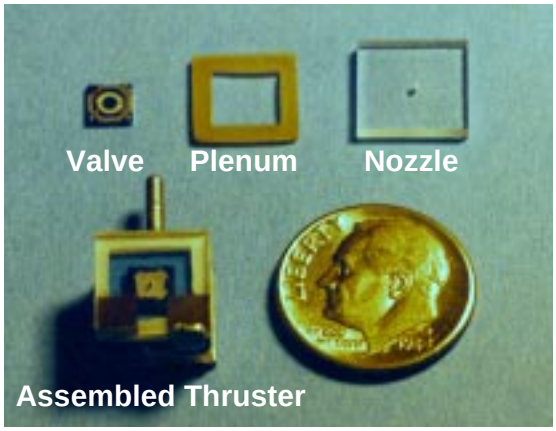

Figure 5. Bi-directional thruster module composed of MEMS silicon valves and laser-machined parts. *(Aerospace Corp. photo)*

The bi-directional thruster valves had a limited stroke; boss-to-valve seat gaps are typically about 20-microns in the open state, thus introducing flow impedance. In addition, electrothermal valves are sensitive to operating temperature and heat transfer to the fluid that is being controlled. We characterized the bi-directional thruster in a vacuum chamber at 5-milliTorr ambient pressure using an inverted pendulum thrust stand based on a NASA-Lewis design.[31] Thrust measurement accuracy was 0.1-mN and mass flow rate measurement accuracy was 5 x 10^{-8} kg/s. Figure 6 shows thrust as a function of feed pressure and valve voltage using room temperature argon as the propellant. The

silicon valves are normally closed, and they begin opening at applied voltages greater than 4.5 V. For 5-Volt operation, the mass flow rate and hence thrust increase as feed pressure increases up to about 19-psi. At higher feed pressures, the thrust (and mass flow rate) drops due to valve cooling by the propellant. An almost linear thrust vs. feed pressure relationship is obtained at 5.5-Volt operation. The maximum thrust of 1-mN at 24.5-psia feed pressure is about an order-of-magnitude below what the nozzle itself can produce at equivalent feed pressure; the thrust level is limited by viscous losses in the microvalve. Estimated minimum impulse bit, based on the 100-ms valve response time, is 0.1-mN-seconds.

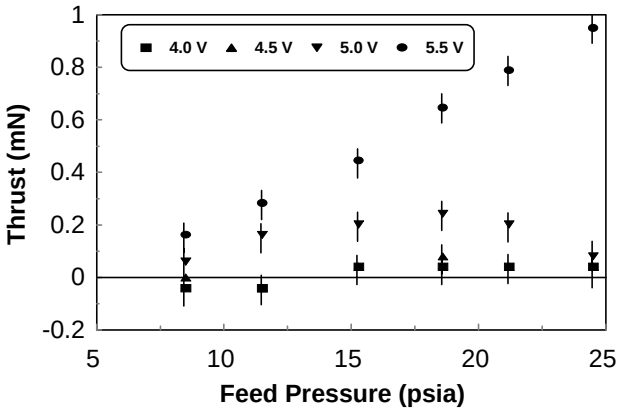

Figure 6. Thrust as a function of feed pressure and valve voltage for the bi-directional cold gas thruster shown in figure 5.

Specific impulse for the bi-directional thruster with argon propellant increased almost linearly from 16-s at 8.5-psia feed pressure to 27-s at 24.3-psia feed pressure. The highest measured specific impulse of 27 s is 50% of the ideal specific impulse for argon with a 10:1 expansion nozzle into a vacuum. Estimated specific impulse using a space-storable low molecular weight propellant such as butane is 37-s. This would support a lifetime velocity increment of 60-m/s with an initial 15% propellant mass fraction. Higher specific impulse can be obtained by using smaller nozzles or by integrating higher flow-rate microvalves such as those described in references 14 and 17.

5. MICROTHRUSTER ARRAYS: "DIGITAL PROPULSION"

TRW, The Aerospace Corporation, and the California Institute of Technology are developing a "digital thruster" under DARPA support.[24] Digital propulsion consists of single-shot thrusters that individually produce only one impulse each; spacecraft maneuvers are performed by firing unused thrusters at specific locations at the right times. Microfabrication enables the creation of large arrays of addressable thrusters, e.g., 10,000 on a 10-cm square surface using 1-mm center-to-center spacing. The digital thruster system is planar, scaleable in area, does not require separate propellant tanks or plumbing, does not require microvalves, and can function as structure. Figure 7 shows a schematic cross-section of the basic concept. The Aerospace Corporation effort has been to design and fabricate thruster components, test various propellants, and characterize thruster performance.

The top ("diaphragm") layer is a 400-micron-thick silicon die, which has a 0.5-micron-thick coating of low-stress silicon nitride on its top and bottom surfaces. Square openings in the top nitride layer are patterned using laser ablation and the bulk silicon is anisotropically etched using potassium hydroxide (KOH). This leaves a 70.6° expansion nozzle of square cross section with a 0.5-micron-thick silicon nitride diaphragm or burst disk on the bottom. Burst pressures of about 200-psi are achieved using a 500-micron-square diaphragm.

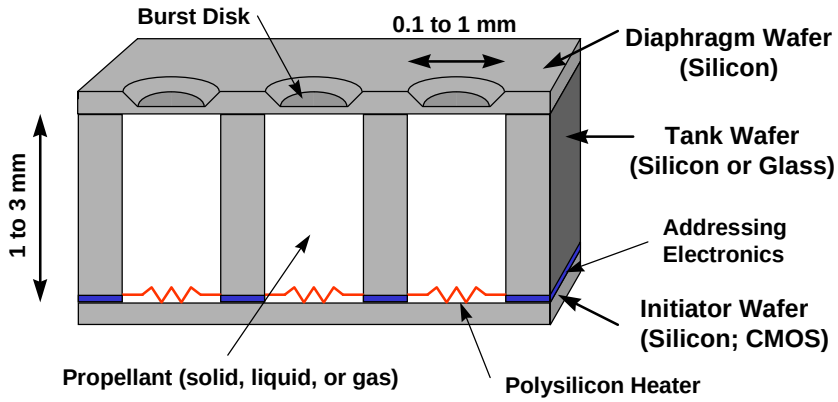

Figure 7. Schematic cut-away view of a "digital" propulsion system.

The middle "tank", or propellant storage layer, is 1-mm-thick Foturan™ which is direct-write laser-exposed, baked to a semi-ceramic state, and then etched in a 5% HF solution in water at 40 degrees C to leave cylindrical cavities. We have fabricated cavities ranging from 300-to-800-microns in diameter on 1-mm centers with little difficulty. Non-circular cross sections (hexagonal, square, star, etc.) can also be fabricated to improve propellant packing efficiency or to control burn characteristics.

The bottom "initiator" layer is a 6-mm-square silicon die that has a 3-micron-thick layer of thermally-grown oxide, a 0.5 or 1-micron thick patterned polysilicon layer, and a 0.35-micron thick metal layer on top. The oxide serves as a transient thermal insulator, the polysilicon traces are 100-Ohm resistors that can also serve as exploding bridge wires, and the metal traces serve as electrical interconnects.

Figure 8 shows an assembled three-layer "rocket chip" mounted in a 24-pin ceramic dual inline package (DIP). The current thruster system consists of 15 solid propellant thrusters in a 3 by 5 array plus four extra outboard nozzles that serve as alignment ports for assembly. A potential of 100-V applied across a 100-Ohm polysilicon resistor (1-micron-thick by 20-microns-wide by 400-microns long) causes it to promptly vaporize, thus generating a pressure wave that ignites lead styphnate, a primary explosive.

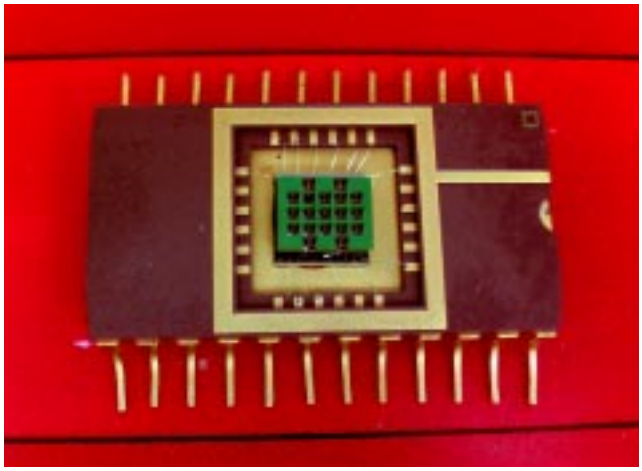

Figure 8. Photograph of an assembled "rocket chip" in a 24-pin ceramic carrier. *(Aerospace Corp. photo)*

We have measured impulse bits produced by our solid rocket digital microthrusters using a ballistic pendulum. Figure 9 shows measured impulse bits, in air, for 8 successive thrusters on a single 15-thruster die. The error bars are due to random pendulum vibrations caused by air currents and the scatter in the data is probably due to variations in propellant mass between thrusters. The solid microthrusters have a blow-down of approximately one millisecond. Each thruster contains roughly 1 milligram of propellant and the expected impulse bit in air is 1.8 mN-s. The measured impulse bits are 5% of expected, and further investigation has revealed that most of the propellant is blown out of the thrusters in an unburned state. We are now investigating the use of smaller propellant particles and smaller diaphragm areas (burst pressures increase to 1000 psi) to promote faster propellant combustion. We are also investigating the use of igniters on the diaphragm side of the propellant cylinder to start combustion near the exit plane.

Figure 9. Measured impulse bits generated by 8 thrusters from a single thruster chip.

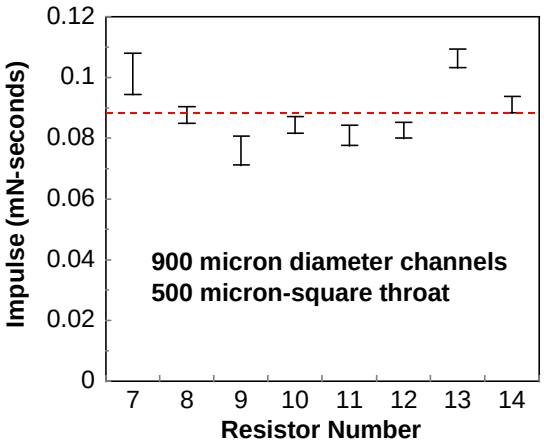

6. CMOS MICRORESISTOJETS

Complimentary metal oxide semiconductor (CMOS) circuits are pervasive in today's world; they are used in computers, wireless telephones, most "smart" appliances, automobiles, etc. A large number of CMOS "foundries" exist, and a fair number are available for custom circuit fabrication. In addition, CMOS processes can be used to produce MEMS if the dice are designed such that selected regions of the silicon substrate are exposed after fabrication. Normally, several layers of dielectric material, metal conductors, and polysilicon cover the silicon base die, topped by a final patterned dielectric layer that prevents contamination of all underlying layers.

Liquid etchants such as HNO_3 and HF in water or acetic acid attack all exposed silicon or polysilicon equally and can be used to undercut dielectric or metal areas. Etch rates vary from about 1-to-10 microns per minute. Liquid etchants such as KOH-water,[32,33] hydrazine-water,[34,35] ethylenediamine-pyrocatechol-water (EDP),[36,37] or tetramethyl-ammonium hydroxide (TMAH)[38,39] attack the <111> planes of silicon at a much slower rate than the other planes to produce "chiseled" cuts as shown in figure 10. These cuts follow the <111> planes that form a 54.7^o angle with the surface for an <100>-oriented silicon substrate typically used for CMOS fabrication. Note that dielectric and metal structures can be completely undercut as shown in Fig. 10D, leaving a suspended structure that is effectively thermally-isolated from the substrate. Reference 40 provides historical information on anisotropic etching to create useful devices, while reference 41 points to an on-line address where one can download a Windows™ program called ACES (Anisotropic Crystalline Etch Simulator) that simulates and graphically displays the etching process. Anisotropic etch rates are typically about 1 micron per minute and in practice, EDP and TMAH are typically used for bulk micromachining of

CMOS dice. These etchants remove silicon at high rate, but not the passivation layers or exposed metals (e.g., bond pads).

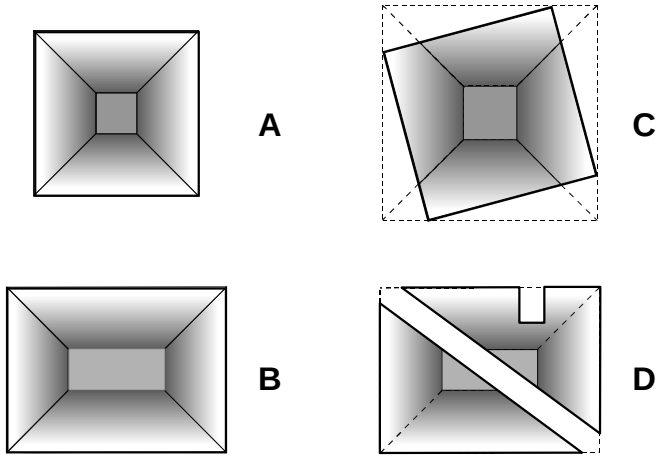

Figure 10. Schematic top view of aniostropic etch pits in silicon: A) Square opening aligned with <111> traces, B) Rectangular opening aligned with <111> traces, C) Square opening not aligned with <111> traces, and D) Bridge and cantilever beam patterns.

The key to cost-effective development is to utilize in-house facilities or existing prototyping services such as the Metal Oxide Semiconductor Implementation Service (MOSIS), the Multi-User MEMS Processes Service (MUMPS),[42,43] and Sandia's SUMMiT service.[44] MOSIS can provide user-designed CMOS die for under $1000 (Tiny Chips; 4 or 5 copies of roughly 2.2 mm x 2.2 mm die) and MUMPS can provide about 14 copies of user-designed 1-cm-square surface-micromachined die for under $3000. For tested and characterized designs, one can have 20-to-50 identical wafers fabricated by a custom foundry for on-the-order-of $100,000.

Figure 11 shows a photograph of our first CMOS resistojet die fabricated using a 2-micron CMOS process offered by Orbit Semiconductor through MOSIS. This "Tiny Chip" is 2.3 mm on a side. The polysilicon layer, normally used as the gate structure in CMOS transistors, was patterned to provide a resistive heater element sandwiched between 2 patterned passivation (glass) layers. This basic concept is an extension of the readily available "pixel-160x160" microheater design developed by the National Institute of Standards and Technology (NIST).[45] Two NIST microheaters were included on the die (center, bottom of figure 11) to test our post-processing technique. Two square openings, one above each microheater in figure 11, were added as an etch-depth indicator. When the square openings become pyramidal pits whose walls meet at a point, the etch process is complete. Resistojet 0 is just the NIST design with an added input channel and an expansion nozzle while Resistojet 1 is a larger design with a heftier heating element. Complete resistojets are created by etching the die to create flow channels, sectioning the die to separate the 4 resistojet sub-die, and bonding paired components together along their broad surfaces.

Figure 11. Photograph of an unetched silicon die with resistojet and electronic structures as received from MOSIS. *(Aerospace Corp. photo)*

Figure 12 shows an SEM of part of the post-etched CMOS silicon die that contains the NIST microheaters on the right and the etch-depth indicators on the left. The polysilicon heating elements are encased in glass films and are suspended above the pyramidal pits by glass and metal stringers; metal traces exit the central heating element and connect to bond pads on the far right.

Figure 12. SEM photograph of EDP-etched structures in a CMOS-processed silicon die. *(Aerospace Corp. photo)*

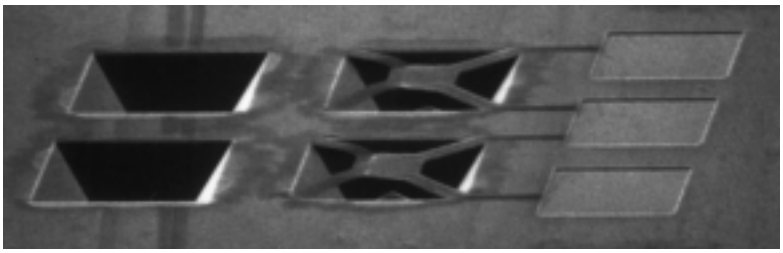

Figure 13 shows a design for third-generation, 3-Watt CMOS resistojet that includes an integrated flow sensor and power transistor.[46] Flow sensing is accomplished using a CMOS microbridge structure, similar to the microheater structure shown in Fig. 12, that emulates a hot wire anemometer.[47] Two polysilicon resistors, one upstream and one downstream, are co-fabricated on a common trampoline structure just upstream of the plenum. Resistance of the downstream polysilicon element is monitored as a function of upstream resistor power.

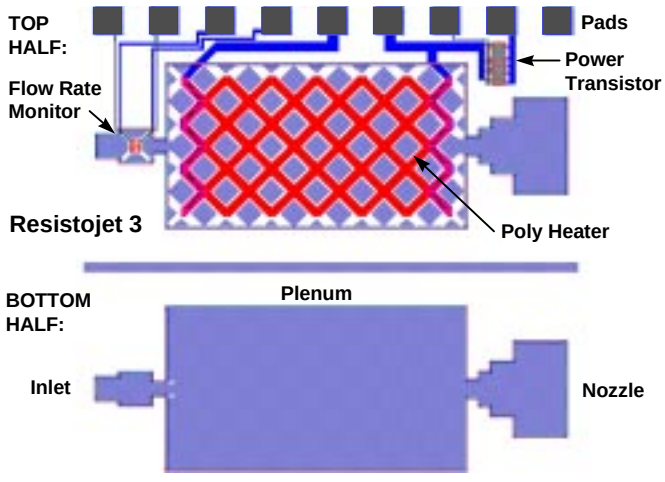

Figure 13. 3-Watt CMOS resistojet designed for a 2.2 mm-square die.

Fig. 14 shows an SEM of a CMOS die, fabricated using 1.2-micron rules, that was over-etched using EDP. Careful design (adding metal stringers at pit edges for additional strength) and process control (adjusting etch temperatures to provide reasonable silicon/silicon oxide etch rate ratios) were required to avoid suspended heater breakage. Note that the suspended heater mesh bows downward; the oxide/polysilicon/oxide layers are in compression. We are currently characterizing heater performance under no-flow conditions, and expect to characterize resistojet performance within a few months.

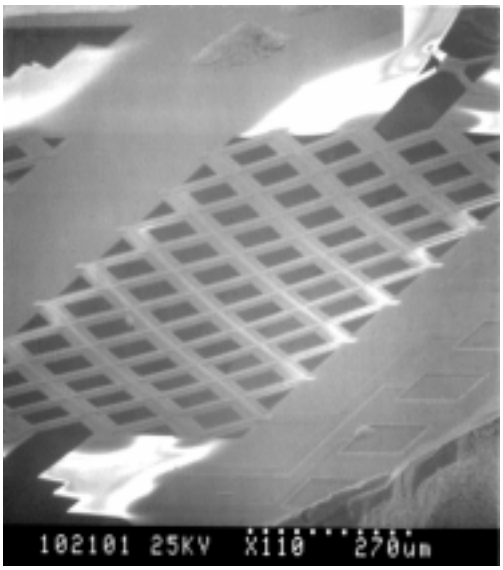

Figure 14. SEM of an over-etched 3-Watt CMOS resistojet die. *(Aerospace Corp. photo)*

7. FIELD ION ENGINES

Field emission, field evaporation, and field ionization are electron tunneling phenomena that require electric fields of 10^7 V/cm and greater. Field emission uses a high electric field to essentially pull electrons out of metals; the applied field diminishes the spatial extent of the local energy barrier enough so that some conduction band electrons can tunnel through and enter free space. The electron current density J is given by the Fowler-Nordheim equation:

$$J = AE^2\Phi^{-1} \exp(-B\Phi^{3/2}/E) \qquad (3)$$

where A and B are constants, E is the electric field strength, and Φ is the work function of the metallic surface.[48] For J in A/cm^2, E in V/cm, and Φ in eV, A is 1.54 x 10^{-6} and B is 6.83 x 10^7.[48] Note that eq. (3) is highly non-linear and that electric fields of 1.8 x 10^7 to 2.5 x 10^7 V/cm are required to generate a 1-mA/cm^2 current density for typical work functions between 4.5 and 3.5-eV. These high fields become possible using modest potential differences of 100-to-1000 Volts if micron-scale and smaller gaps are used between electrodes with textured solid surfaces that exploit field enhancement, e.g., sharp tips or edges of 10-to-100-nm scale.

Field emission sources are currently under development as an enabling technology for flat panel displays, simplified microwave tubes, and vacuum microelectronics.[48,49,50] Examples of field emission sources include Spindt cathodes and diamond-like carbon coatings.[51,52] Spindt cathodes, shown schematically in Fig. (15), are composed of a micron-scale conical emitter centered within a circular aperture of a gate electrode. A "formed" (extra sharp emitters produced by thermal field forming) 10,000 tip Spindt cathode array can produce 1 mA electron currents using a potential difference of ~31 Volts.[51] These sources could be used to neutralize the ion beam from a micromachined ion engine. A 1-Watt ion engine suitable for nanosatellite primary propulsion operating at a specific impulse of 2000-seconds using xenon would require only 2.5-mA of neutralizing electrons and a Spindt cathode array area of only 0.02-mm^2 using a 1-micron pitch with hexagonal packing.

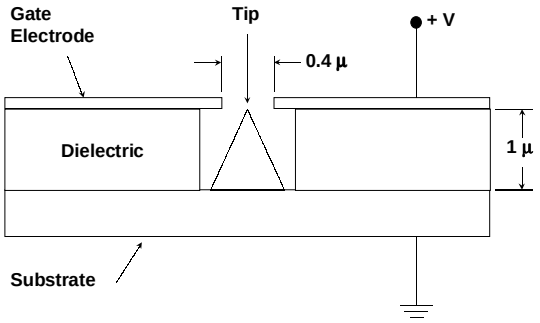

Figure 15. Schematic cross-section of the Spindt cathode.

Field evaporation/ionization sources using liquid anodes are readily available as high-brightness liquid metal ion sources. These devices exploit the instability of conducting liquid surfaces when electric fields of 10^5 to 10^6 V/cm are applied.[53] Electrodynamic forces cause the liquid surface to form one or more Taylor[54] cones that have sharp tips with radii-of-curvature between 5 and 50 nm, thus generating local electric fields in excess of 10^7 V/cm through field enhancement. The Field Emission Electric Propulsion (FEEP) thruster is an existing micronewton class electrostatic thruster that operates at specific impulses in the 6000 to 10,000+ s range.[55] This particular device uses cesium in a planar slit geometry that is manufactured using conventional machining techniques. A single-tip liquid indium ion source suitable for use as a ~1-Watt, ~10-μN ion thruster has successfully operated on-orbit.[56] One disadvantage of the FEEP and liquid indium source is that ion extraction energies of 5-to-10 kV are required due to macroscopic anode-extractor gap widths; lower voltage and hence lower specific impulse operation will require microscopic gaps to increase local electric field strength.

Johannes Mitterauer proposed miniaturized liquid metal ion sources (MILMIS) that could be fabricated using microfabrication technology in the early 1990's.[57,58] These devices were based on the Spindt "microvolcano" which is basically a reverse-polarity Spindt cathode with a hole drilled through the emitter to feed gas or liquid to the high-field region near the gate.[51] The advantage of this microfabrication approach is that required gross electric fields of 10^6 V/cm may be readily generated by applying one hundred Volts across a 1-micron-wide gap. Since the field evaporation/ionization process is fairly efficient (less than 10 eV loss per ion), ion engines with high thrust efficiency at low specific impulse, e.g., 1300 s for indium, become possible. The main disadvantage is the use of liquid metal propellants, e.g., possible spacecraft contamination and the thermal losses associated with maintaining the propellant in a molten state.

Field ionization, which is exploited in the field ion microscope, can also be used to ionize gaseous propellants.[59] Equation (4) gives the maximum barrier penetration probability P of the electron in the atom at a critical distance, χ_c, near the surface of a conductor: [60]

$$P(\chi_c,F) = exp\{-0.683(I - 7.59F^{1/2})^{1/2}\,[(I-\phi)/F]\} \qquad (4)$$

where I is the ionization potential of the atom or molecule in electron volts, ϕ is the work function of the surface in electron volts, and F is the applied field in units of Volts/Å. The probability approaches unity for xenon (I = 12.1 eV) near tungsten (ϕ = 4.5 electron volts) at an applied field F of 2.5 V/Å (2.5 x 10^8 V/cm). The critical distance χ_c exists because the electron must have some place to go; it cannot enter a filled electronic state in the metal. The critical distance χ_c is approximately given by

$$\chi_c = (I - \phi) / F \qquad (5)$$

where χ_c is in Å; about 3 Å for the xenon-tungsten system at 2.5 V/Å. Within the critical distance, the ionization probability becomes zero because tunneling is no longer allowed.

Since electrodynamic flow into sharp tips cannot be exploited using gaseous propellants, nanostructured electrodes with edges or tips of 5-to-50 nm radius must be used. In addition, neutral propellant atoms or molecules must have a very high probability of approaching high field regions to within the critical distance without leaving the system. Once an ion is formed, it should have a high probability of accelerating away from the anode and leaving the system without colliding with neutrals. These contradictory requirements can be met using free molecular flow conditions between the electrodes and small exit apertures or baffles for ion escape.

Figure 16 shows a cross-sectional view of one possible concept that uses multiple ion acceleration channels. Gas is fed into the lower plenum and can escape only by exiting through the 1-micron diameter holes in electrodes 1 and 2. With micron-thick dielectric layers, free-molecular flow conditions can exist at relatively high (~10-Torr) plenum pressures, thus creating a low conductance path for neutral escape. Electrode 1 is biased on-the-order-of 100 Volts more positive than electrode 2 to create field ionization around the sharp upper edges of electrode 1 orifices. This potential difference controls the ion production rate for a fixed geometry. Electrode 3 is at spacecraft potential and can be more positive or negative than electrode 2 depending on the desired specific impulse. Field ionization allows molecular ionization without high levels of fragmentation, which may enable use of space-storable propellants over a wide molecular weight range to further broaden the specific impulse envelope.

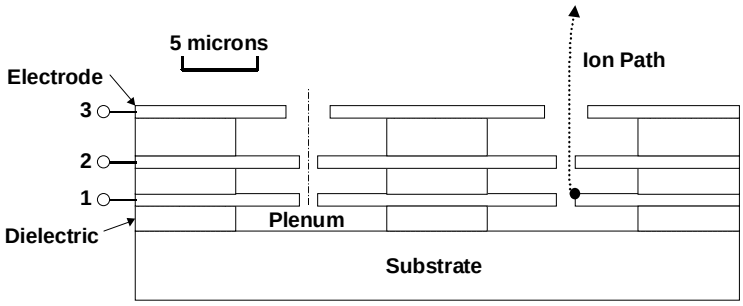

Figure 16. A micromachined ion engine concept based on field ionization. Electrode 1 is the field emission electrode, electrode 2 is the gate electrode, and electrode 3 is the decel/accel electrode. Two cylindrical symmetric engine channels are shown.

A number of fabrication and operational issues such as dimensional control, dielectric breakdown strength, fabrication of nanostructured components, and lifetime of nanostructured surfaces need to be addressed before a prototype field ionization thruster can be demonstrated. We designed several field emission and field ionization test structures, within the limitations of a conventional CMOS process, before trying to develop customized fabrication techniques. These structures were part of a Tiny Chip die, shown in Fig. 17, which was manufactured using a 2-micron CMOS process available through MOSIS. By applying a timed hydrofluoric acid etch to remove 3 linear microns of glass, the exposed glass passivation layers will be removed along with part of the layers that are sandwiched between metal, polysilicon, or silicon. Metal and polysilicon structures that are thinner than 6 microns in any direction parallel to the surface will be completely undercut while larger features will retain some glass to mechanically anchor them in place. The field emission wires shown in Fig. 17 are 4-micron-wide features composed of metal1, metal2, or polysilicon that are electrically isolated from the substrate or conducting layer below (gate electrode) and electrically connected to bond pads at each end. These structures will be tested as field emission sources by biasing the “wires” negative with respect to a gate electrode below. The gap between the “wire” and the gate electrode varies from 0.6 to 1.9-microns.

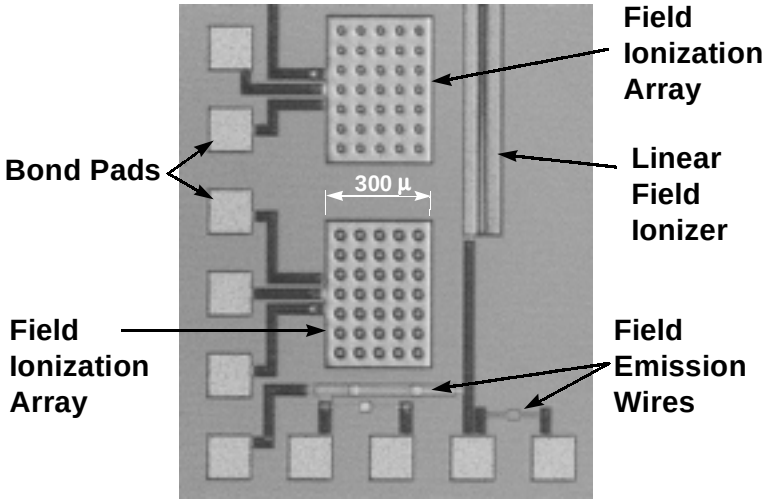

Figure 17. Photograph of one corner of a CMOS die that contains several field-ionization grid structures and thermionic filaments. *(Aerospace Corp. photo)*

Figure 18 shows the expected schematic cross section of one of the field ionizer channels after etching. These structures will be tested for breakdown field strength between the metal and polysilicon layers under vacuum and at various pressures up to 10-Torr. The field oxide between the substrate and the polysilicon layer is 0.6-microns thick, the glass layer between the polysilicon and metal1 layers is 0.9-microns thick, and the glass layer between the metal1 and metal2 layers is 1.1-microns thick. If 10^6 V/cm can be established between planes (about 100 Volts between layers), these structures will be tested for field ionization capability under 10-Torr ambient pressure of atomic (argon, xenon, etc.) and molecular propellants.

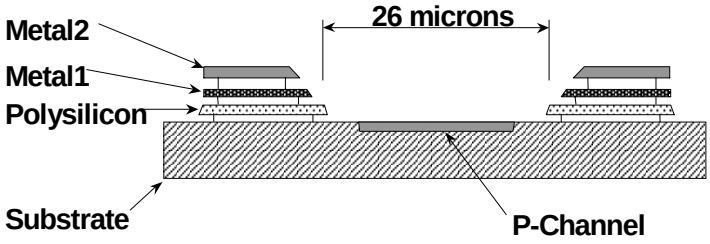

Figure 18. Cross-sectional view of a micro field ionization test structure after etching.

8. SUMMARY

Nanosatellites are highly integrated 1-to-1000 gram mass spacecraft that could be mass-produced using semiconductor and microelectromechanical systems (MEMS) batch-fabrication techniques. Using this approach, unique space architectures that use thousands of small spacecraft become possible. One new approach is to use hundreds or thousands of spacecraft in a rotating disk geometry that can be used as a sparse aperture antenna with kilometer-scale diameters. In general, nanosatellites will require microthrusters with micro-to-millinewton thrust levels for orbit insertion, orbit maintenance, disposal, and attitude control.

While some types of thrusters may not scale down efficiently to sub-millinewton thrust levels, new devices based on sub-micron structures become possible. At Aerospace, we have fabricated two chemical microthrusters using a combination of laser-machining and semiconductor fabrication techniques: a 0-to-1 mN thrust bi-directional cold gas microthruster and a novel array of single-shot

microthrusters. The latter effort is part of an on-going MEMS effort supported by DARPA. Impulse bits of 0.1 mN-s were produced by individual microthrusters in the batch-producible array using lead styphnate as a solid chemical propellant. We are also investigating the use of CMOS semiconductor fabrication techniques for constructing microresistojets and field emission-based micro ion engines. Various test devices have been fabricated, but actual thrust measurements have not yet been attempted.

Acknowledgments

We gratefully acknowledge the support provided by the Aerospace Corporation through the Corporate Research Initiative in MEMS and through the Corporate Strategic Initiative in Nanosatellites. We also gratefully acknowledge DARPA for supporting the "Microsatellite Propulsion and Attitude Control System" MEMS program at TRW, The Aerospace Corporation, and the California Institute of Technology. Finally, we would also like to thank Ronald Cohen, Meg Abraham, Ruby Robertson, Pete Fuqua, Brian Brady, Ed Beiting, Jim Pollard, and "George" Chao at the Aerospace for their efforts in fabricating and testing various microthruster components and systems, and in analyzing formation-keeping propulsion requirements.

1 H. Helvajian, editor, Microengineering Technology for Space Systems, ISBN 1-884989-05-5, Aerospace Press, El Segundo, CA, and AIAA, Reston, VA, 1995.

2 H. Helvajian and E.Y. Robinson, editors, Micro- and Nanotechnology for Space Systems, ISBN 1-884989-04-7, Aerospace Press, El Segundo, CA, and AIAA, Reston, VA, 1993.

3 H. Helvajian, editor, Microengineering for Aerospace Systems, ISBN 1-884989-03-9, Aerospace Press, El Segundo, CA, and AIAA, Reston, VA, 1999 (in press).

4 W.C. Tang, "Micromechanical Devices at JPL for Space Exploration," IEEE 1998 Aerospace Conference, Aspen, Colorado, March 21-28, 1998.

5 H. Helvajian, S. Janson, and E.Y. Robinson, "Big Benefits from Tiny Technologies: Micro-Nanotechnology Applications in Future Space Systems," p. 3-34 in Advancement of Photonics for Space, edited by E.W. Taylor, CR66, Critical Reviews of Optical Science and Technology, SPIE Press, Bellingham, WA, 1997.

6 A.M. de Aragon et al., Micro/Nano-Technologies for Space, Round Table at ESTEC, European Space Agency Report ESA WPP-091, March 1995.

7 Proceedings of the International Conference on Integrated Micro/Nanotechnology for Space Applications in Houston, Texas, Oct. 30 -Nov. 3, 1995, Aerospace Press, El Segundo, CA.

8 J.G. Walker, "The Geometry of Satellite Clusters," Journal of the British Interplanetary Society, Vol. 35, pp.345-354, 1982.

9 J. Murdoch and J.J. Pocha, "The Orbit Dynamics of Satellite Clusters," International Astronautics Federation paper IAF-82-54.

10 Chobotov, V.A., editor, Orbital Mechanics, Second Edition, AIAA Education Series, 1996, pp.259-264.

11 C.C. Chao, J.E. Pollard, and S.W. Janson, "Dynamics and Control of Cluster Orbits for Distributed Space Missions," paper AAS 99-126, Proceedings of the 9th AAS/AIAA Space Flight Mechanics Meeting, Breckenridge, Colorado, Feb 7-10, 1999.

12 T.S.J. Lammerink, M. Elwenspoek, and J.H.J. Fluitman, "Integrated Micro-Liquid Dosing System," p. 254-259, Proc. IEEE Micro Electro Mechanical Systems Workshop, Fort Lauderdale, Florida, February, 1993.

13 R. Zengerle et al., "A Micro Membrane Pump with Electrostatic Actuation," Proc. IEEE Micro Electro Mechanical Systems Workshop, p.19-24 1992.

14 A.K. Henning, "Microfluidic MEMS," IEEE 1998 Aerospace Conference, Aspen, Colorado, March 21-28, 1998.

15 H. Baltes, O. Paul, and O. Brand, "Micromachined Thermally Based CMOS Microsensors," Proceedings of the IEEE, 86 # 8, pp.1660-1678, August 1998.

16 D. Maillefer, H. van Lintel, G. Rey-Mermet, and R. Hirschi, "A High-Performance Silicon Micropump for an Implantable Drug Delivery System," Proceedings of the 12th IEEE International Conference on Micro Electro Mechanical Systems, Orlando, Florida, Jan. 17-21, 1999.

17 C. Grosjean, X. Yang, and Yu-Chong Tai, "A Practical Thermopneumatic Valve," Proceedings of the 12th IEEE International Conference on Micro Electro Mechanical Systems, Orlando, Florida, Jan. 17-21, 1999.

18 J. Mueller, "Thruster Options for Microspacecraft: A Review and Evaluation of Existing Hardware and Emerging Technologies," AIAA paper 97-3058, Seattle, WA, July 1997.

19 S.W. Janson and H. Helvajian, "Batch-Fabricated Microthrusters for Kilogram-Class Spacecraft," Government Microcircuits Applications Conference (GOMAC), Arlington, Virginia, March 1998.

20 W.A. deGroot and S.R. Oleson, "Chemical Microthruster Options," AIAA paper 96-2863, Lake Buena Vista, FL, July 1996.

21 Proceedings, JPL Micropropulsion Workshop, JPL, Pasadena, CA, April 7-9, 1997.

22 J. Mueller et al., "Design, Analysis, and Fabrication of a Vaporizing Liquid Micro-Thruster," AIAA paper 97-3054, Seattle, WA, July 1997.

23 R.L. Bayt, A.A. Ayon, and K.S. Breuer, "A Performance Evaluation of MEMS-based Micronozzles," AIAA paper 97-3169, Seattle, WA, 1997.

24 D.H. Lewis, S.W. Janson, R.B. Cohen, and E.K. Antonsson, "Digital Micropropulsion," Proceedings of the 12th IEEE International Conference on Micro Electro Mechanical Systems, Orlando, Florida, Jan. 17-21, 1999.

25 R. Bayt and K.S. Breuer, "Viscous effects in supersonic MEMS-Fabricated micronozzles," Proceedings of the 3rd ASME Microfluids Symposium, Anaheim, CA, Nov. 1998.

26 Hydrazine Handbook, p. 2-7 and 2-8, Rocket Research Company (now Primex), Redmond, WA.

27 Francis F. Chen, Introduction to Plasma Physics, First Edition, pp. 169-173, Plenum Press, New York, 1974.

28 G.J. Yashko, G.B. Giffen, and D.E. Hastings, "Design Considerations for Ion Microthrusters," paper 97-072, Proceedings of the 25th International Electric Propulsion Conference, Cleveland, Ohio, Aug. 24-27, 1997.

29 W.W.Hansen, S.W.Janson, and H.Helvajian, "Direct-Write UV Laser Microfabrication of 3D Structures in Lithium-Alumosilicate Glass," SPIE Proc. Vol. 2991, pg. 104 (1997).

30 D. Hülsenberg, R. Bruntsch, K. Schmidt, and F. Reinhold, Mikromechanische Bearbeitung von fotoempfindlichem Glas, Silikattechnik, Vol. 41 p. 364, (1990).

31 T.W. Haag, "Thrust Stand for High-Power Electric Propulsion Devices," Rev. Sci. Instrum. 62 (5), p. 1186 (1991).

32 K.D. Bean, "Anisotropic Etching of Silicon," IEEE Transactions on Electron Devices, p. 1185, ED-25, 1978.

33 A.I. Stoller, "The Etchining of Deep, Vertical-Walled Patterns in Silicon," RCA Review, p. 271, 31, 1970.

34 D.B. Lee, "Anisotropic Etching of Silicon," J. Appl. Phys., p. 4569, 40, 1969.

35 M. Declerq, L. Gerzberg, and J. Meinol, "Optimization of the Hydrazine-Water Solution for Anisotropic Etching Silicon in Integrated Circuit Technology," J. Electrochem. Soc., p. 545, 122, 1975.

36 A. Reisman et al., "The controlled Etching of Silicon in Catalyzed Ethylenediamine-Pyrocatechol-Water Solutions," J. Electrochem. Soc., p.1406, 126, 1979.

37 M.P. Wu, Q.H. Wu, and W.H. Ko, "A Study on Deep Etching of Silicon Using Ethylenediamine-Pyrocatechol-Water," Sensors and Actuators, p. 333, 9, 1986.

38 O. Tabata et al., Technical Digest, Transducers '91; IEEE Int. Conf. On Solid-State Sensors and Actuators, p. 811, 1991.

39 U. Schnakenberg, Technical Digest, Transducers '91; IEEE Int. Conf. On Solid-State Sensors and Actuators, p. 815, 1991.

40 J.B. Angell et al., "Silicon Micromechanical Devices," Scientific American, p.44-55,248, #4, April 1983.

41 Microactuators, Sensors, and Systems Group, University of Illinois at Urbana-Champaign, Availabe on-line: http://galaxy.ccsm.uiuc.edu/aces

42 The MOSIS Service, Information Sciences Institute, University of Southern California. Available on-line: http://www.isi.edu/mosis

43 The MUMPS Service, MEMS Technology Applications Center, 3021 Cornwallis Road, Research Triangle Park, NC Available on-line: http://mems.mcnc.org/mumps.html

44 The Sandia Summit Service, Sandia National Laboratories, Albquerque, NM Available on-line: http://www.mdl.sandia.gov/Micromachine/trilevel.html

45 J. Marshall et al., "Realizing Suspended Structures on Chips Fabricated by CMOS Foundry Processes Through the MOSIS Service," NIST report NISTIR 5402, June 1994. Available on-line: http://www.mosis.org/pubs

46 S.W. Janson, "Batch-Fabricated Resistojets: Initial Results," Paper 97-070, International Electric Propulsion Conference, Cleveland, Ohio, Sept. 1997.

47 W. Allegretto, "Modeling and Simulation of Microsensors and Actuators," Chapter 2 in Sensor Technology and Devices, Ljubisa Ristic (ed), pp.36-39, Artech House, Norwood, MA, 1994.

48 S. Iannazzo, "A Survey of the Present Status of Vacuum Microelectronics," 36, #3, pp.301-320, 1993.

49 K.L. Jensen, R.H. Abrams, and R.K. Parker, "Field Emitter Array Development for High Frequency Applications," Journal Vac. Sci. Technol. B, 16 #2, pp. 749-753, 1998.

50 C.A. Spindt, C.E. Holland, P.R. Schwoebel, and I. Brodie, "Field Emitter Array Development for Microwave Applications: II," Journal Vac. Sci. Technol. B, 16 #2, pp. 758-761, 1998.

51 C.A. Spindt, "Microfabricated field-emission and field-ionization sources," Surface Science, 266, pp.145-154, 1992.

52 S.J. Kwon, Y.H. Shin, D.E. Aslam, and J.D. Lee, "Field Emission Properties of the Polycrystalline Diamond Film Prepared by Microwave-Assisted Plasma Chemical Vapor Deposition," Journal Vac. Sci. Technol. B, 16 #2, pp. 712-715, 1998.

53 G.N. Fursey, L.A. Shirochin, and L.M. Baskin, "Field-Emission Processes From a Liquid Metal Surface," Journal Vac. Sci. Technol. B, 15 #2, pp. 410-421, 1997.

54 G.I. Taylor, "Disintegration of Water Drops in an Electric Field," Proc. Roy. Soc., A280, p.313, 1964.

55 S. Marcuccio, A. Genovse, and M. Andrenucci, "Experimental Performance of Field Emission Microthrusters," Journal of Propulsion and Power, 14, #5, pp.774-780, 1998.

56 M. Fehringer, F. Rudenauer, and W. Steiger, "Space-Proven Indium Liquid Metal Field Ion Emitters for Ion Microthruster Applications," AIAA 97-3057, 33rd AIAA/ASME/SAE/ASEE Joint Propulsion Conference, Seattle, WA, July 6-9, 1997.

57 J. Mitterauer, "Miniaturized Liquid Metal Ion Sources (MILMIS)," p. 790-799, IEEE Transactions on Plasma Science, 19, #5, Oct 1991.

58 J. Mitterauer, "Prospects of Liquid Metal Ion Thrusters for Electric Propulsion," IEPC paper 91-105, 22nd AIDAA/AIAA/DGLR/JSASS International Electric Propulsion Conference, Viareggio, Italy, Oct 1991.

59 T. T. Tsong, Atom-Probe Field Ion Microscopy, Cambridge University Press, 1990.

60 T. T. Tsong, Atom-Probe Field Ion Microscopy, Cambridge University Press, p. 13, 1990.